CHAPTER 6. DISCUSSION

In this chapter, the experimental results obtained in this thesis have been analysed and discussed with a global perspective. Three aspects of the fracture and fatigue behaviour have been considered: static residual strength, infinite fatigue life and finite fatigue life.

6.1 Residual strength diagrams

Kitagawa-Takahashi diagram can be extended to the static failure occurring at one cycle. In this failure diagram for static loading, the limit in the *MSC* regime is taken as the tensile strength, σ_t, and the prediction for *LC* regime is calculated with the fracture toughness, K_{IC}, being the allowable nominal stress given by:

$$\sigma = \frac{K_{IC}}{\sqrt{\pi a}} \tag{6-1}$$

El Haddad model is also suitable for this static case, introducing the characteristic length, l_0^s, for the static response:

$$\sigma_{Hd} = \frac{K_{IC}}{\sqrt{\pi\left(a + l_0^s\right)}} \tag{6-2}$$

where:

$$l_0^s = \frac{1}{\pi}\left(\frac{K_{IC}}{\sigma_t}\right)^2 \tag{6-3}$$

Figure 6-1. Residual strength diagrams including modified Kitagawa-Takahashi (continuous line) and El Haddad predictions (dashed line) of: a) SLS PA-12 at 0° orientation b) SLS PA-12 at 90° orientation and c) IM PA-12. Experimental data obtained from fracture tests and tensile tests carried out in plain specimens and samples with small and medium-size cracks are included as filled orange circles.

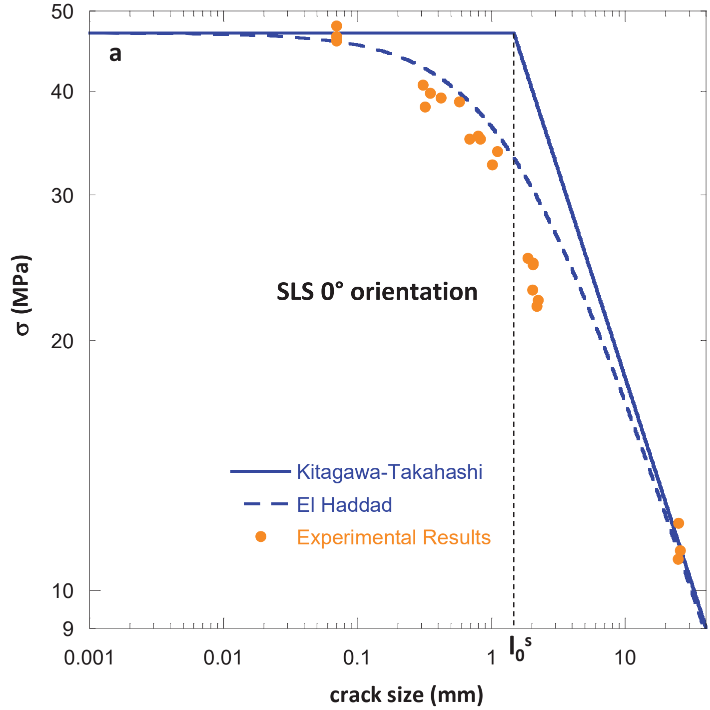

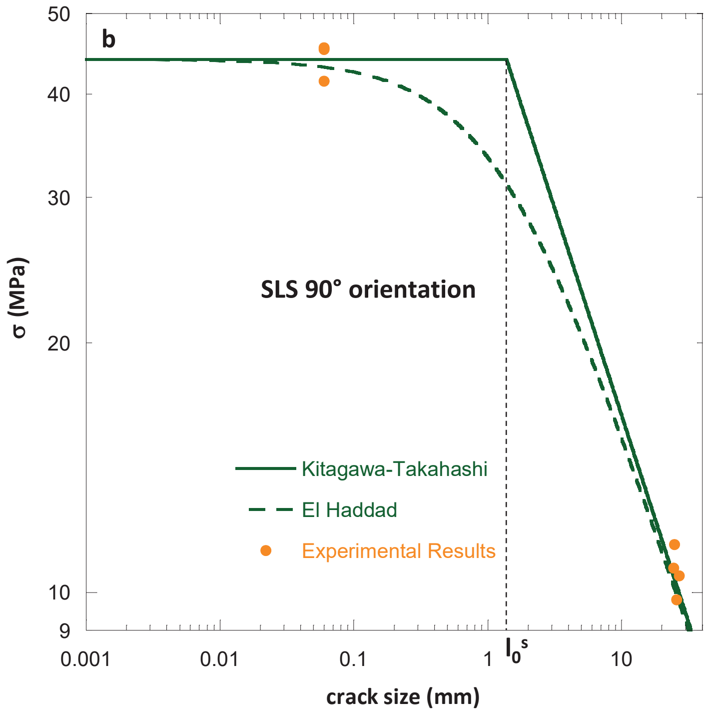

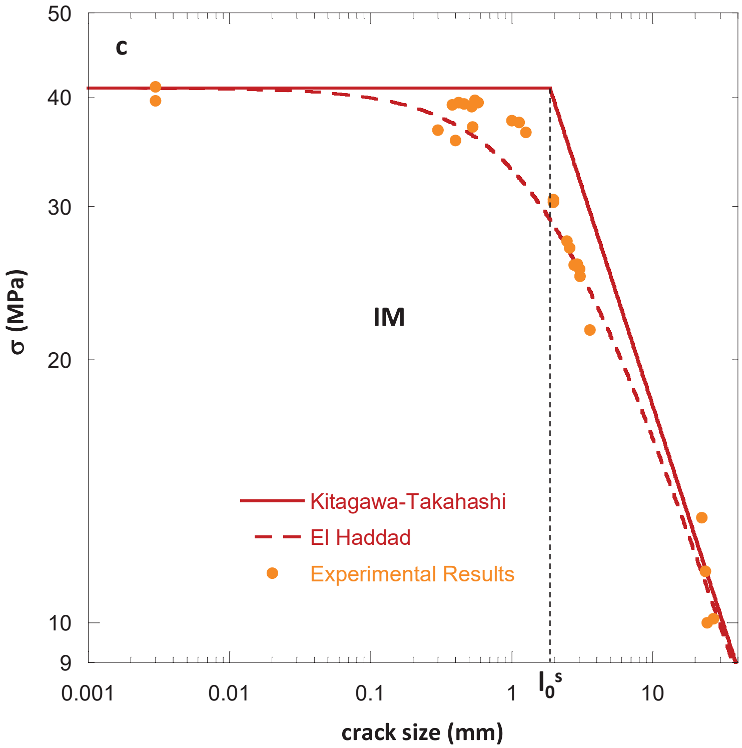

Figure 6-1 shows the residual strength curves, in continuous line, and the modified El Haddad model, in dashed line, of *SLS* PA-12 at 0° and at 90° orientations and of *IM* PA-12.

Experimental data from tensile tests and fracture tests presented in *sections 5.5* and *5.6*, respectively, were also included. The former was assigned a defect of equal size to the surface roughness shown in *section 5.2*. The diagrams were completed with the results obtained from monotonic loading tests carried out in specimens with small and medium-size crack lengths in the range between 0.2 and 3 mm for *SLS* at 0° orientation and for *IM* PA-12.

Figure 6-2 Residual strength diagrams including modified Kitagawa-Takahashi (continuous line) and El Haddad predictions (dashed line) for static loading of SLS PA-12 at 0° orientation (blue), SLS PA-12 at 90° orientation (green) and IM PA-12 (red).

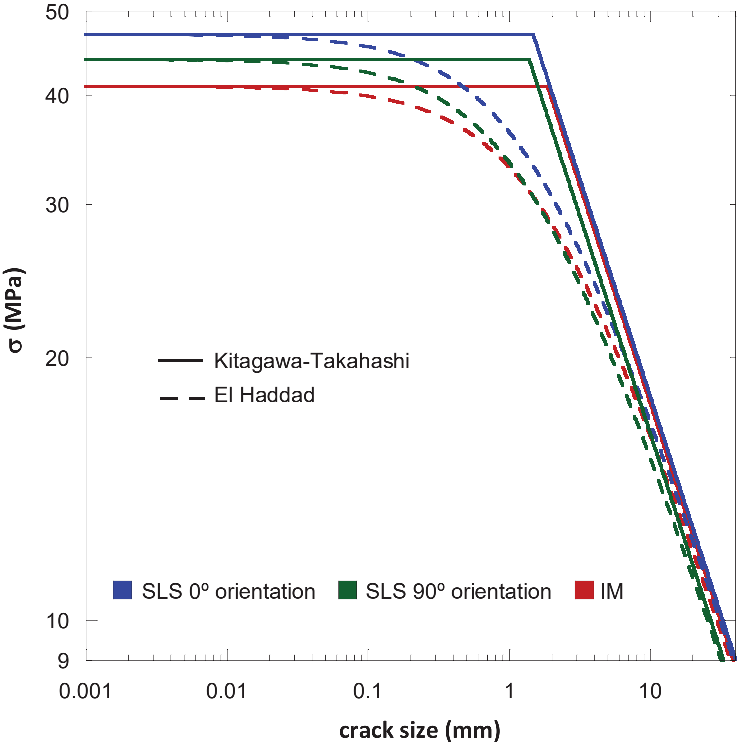

To get an easier visual comparison of the materials, *Figure 6-2* displays the three residual strength curves for static loading all together. *SLS* PA-12 in the *MSC* regime shows higher allowable stresses, due to their higher tensile strengths, but the three materials present similar behaviours at *LC* regime. Differences in l_0^s for each material are also distinguished.

The characteristic static lengths l_0^s are shown in *Table 6-1*. As it can be seen, both *SLS* PA-12 orientations have a similar l_0^s value, which is clearly smaller than that of *IM PA-12*.

A normalized diagram may help to unify all the results corresponding to different materials in just one curve. *Figure 6-3* contains the same information as the three curves presented in *Figure 6-1* but, in this case, the Y-axis was

Table 6-1. Characteristic static length, l_0^s.

Processing technique	Orientation	l_0^s(mm)
SLS	**0° orientation**	1.5
	90° orientation	1.4
IM	**-**	1.9

Figure 6-3. Normalized residual strength diagrams including modified Kitagawa-Takahashi (continuous line) and El Haddad predictions (dashed line) of SLS PA-12 at 0° orientation (blue), SLS PA-12 at 90° orientation (green) and IM PA-12 (red). Experimental data obtained from fracture tests and tensile tests carried out in plain specimens and samples with small and medium-size cracks are included as filled circles.

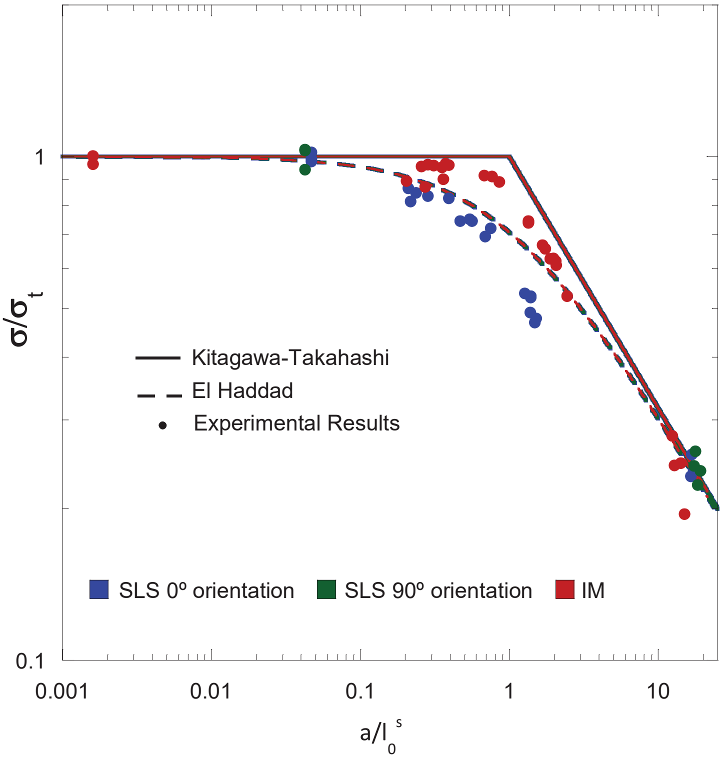

normalized by the tensile stress of each material and the X-axis was also normalized by the l_0^s values contained in *Table 6-1.*

Figure 6-3 displays the prediction capabilities of the empirical models as the modified Kitagawa-Takahashi and El Haddad regarding the static strength of the PA-12 manufactured by different techniques. The diagram is a prediction of the frontier between the integrity and the failure regimes and, consequently, the modified Kitagawa-Takahashi is too conservative. The modified El Haddad model provides better predictions as the experimental data tend to fall on the model curves.

6.2 Infinite fatigue lifetime

The Kitagawa Takahashi diagrams including the predictions of El Haddad model for infinite fatigue lifetime have been constructed from the values of fatigue limit $\Delta\sigma_{fl}$ at 10^6 cycles and crack propagation threshold $\Delta\sqrt{G}_{th}$. As the stress range for infinite fatigue lifetime is calculated from the threshold stress

Figure 6-4. Kitagawa-Takahashi diagram (blue line) including El Haddad empirical model (purple line) of a) SLS PA-12 at 0° orientation, b) SLS PA-12 at 90° orientation and c) IM PA-12.ex Experimental data from $\Delta\sqrt{G}$-decreasing tests are plotted with orange filled circles, and the run-outs and failures of the tests employed for the fatigue limit determination are plotted as diamonds and crosses, respectively.

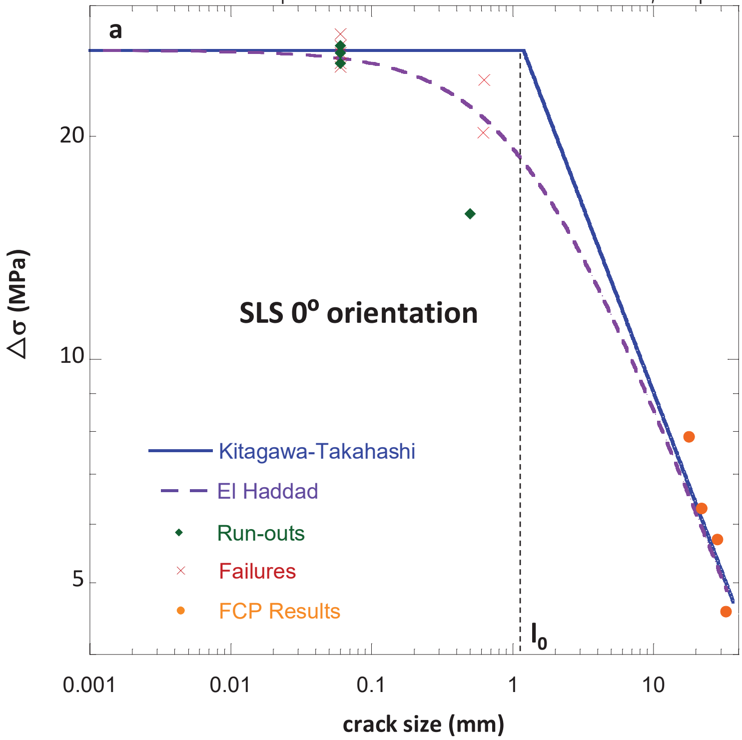

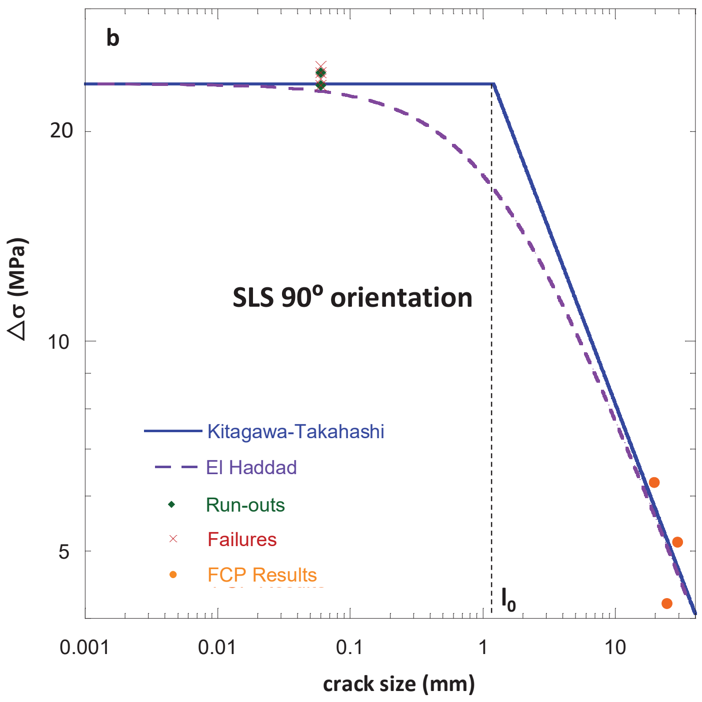
b
20
10
5
Δσ (MPa)
SLS 90° orientation
Kitagawa-Takahashi
El Haddad
Run-outs
Failures
FCP Results
l_0
0.001
0.01
0.1
1
10
crack size (mm)

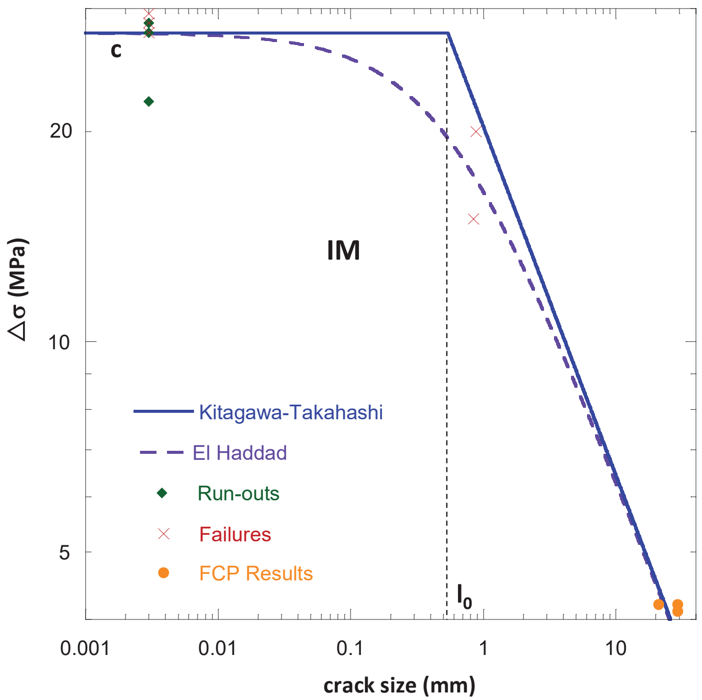
c
20
10
5
Δσ (MPa)
IM
Kitagawa-Takahashi
El Haddad
Run-outs
Failures
FCP Results
l_0
0.001
0.01
0.1
1
10
crack size (mm)

Table 6-2. Characteristic length, l_0, for the materials under study.

Processing technique	**Orientation**	**l_0(mm)**
SLS	**0° orientation**	1.2
	90° orientation	1.21
IM	***IM***	0.54

intensity factor, ΔK_{th} *(eq. (2-4))*, all the data expressed in terms of the control parameter $\Delta\sqrt{G}$ were transformed using the following expression:

$$\Delta K = \Delta\sqrt{G}\sqrt{\frac{2E}{B\frac{dg}{d\alpha}}f(\alpha)} \qquad (6\text{-}4)$$

Figure 6-4 displays the Kitagawa-Takahashi diagrams of *SLS* and *IM* PA-12 specimens. Experimental data from $\Delta\sqrt{G}$-decreasing Fatigue Crack Propagation tests (*FCP* Results) have been depicted with filled orange circles, and the results employed for the calculation of the fatigue limit have been also drawn, the run-outs as diamonds and the failures as crosses. Despite the fatigue life tests were carried out in plain specimens, a defect size was assigned equal to the surface roughness measured and displayed in *section 5.2*. For *SLS* PA-12 at 0° orientation *(Figure 6-4.a)* and for the *IM* PA-12 *(Figure 6-4.c)*, fatigue tests on specimens with small cracks were included.

A characteristic length, l_0, can be obtained from the intersection of *MSC* and *LC* estimations (*equation (2-6))* in the Kitagawa-Takahashi diagrams. This length can be considered as the limiting dimension of a subcritical defect, above which the long crack ΔK_{th} becomes the control parameter. *Table 6-2* shows the values of l_0 for the materials under study. While there are no differences between the characteristic lengths of SLS PA-12 at 0° and 90° orientations, the value of IM PA-12 is much smaller. Comparing the static characteristic length, l_0^s, (*Table 6-1*) and l_0 (*Table 6-2*), the latter is always smaller, ranging the difference from 25% in *SLS* PA-12 up to 300% in *IM* PA-12.

Figure 6-5 displays the Kitagawa-Takahashi diagrams and El Haddad model. As observed, the behaviour of the three materials differ, being *IM* PA-12 the most resistant in the MSC regime.

This could be accounted for the high number of defects in form of pores and unmolten particles present in *SLS* PA-12. On the other hand, in the *LC*

Figure 6-5. Kitagawa-Takahashi diagrams (continuous line) including El Haddad empirical models (dotted line) of SLS PA-12 at 0° orientation (blue), SLS PA-12 at 90° orientation (green) and IM PA-12 (red).

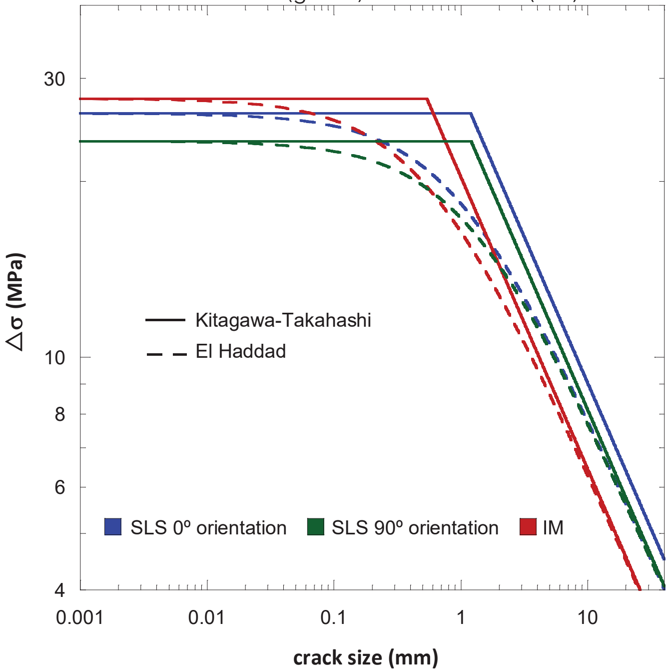

Figure 6-6. Kitagawa-Takahashi diagrams (continuous line) including El Haddad empirical models (dotted line) in normalized coordinates of SLS PA-12 at 0° orientation (blue), SLS PA-12 at 90° orientation (green) and IM PA-12 (red).

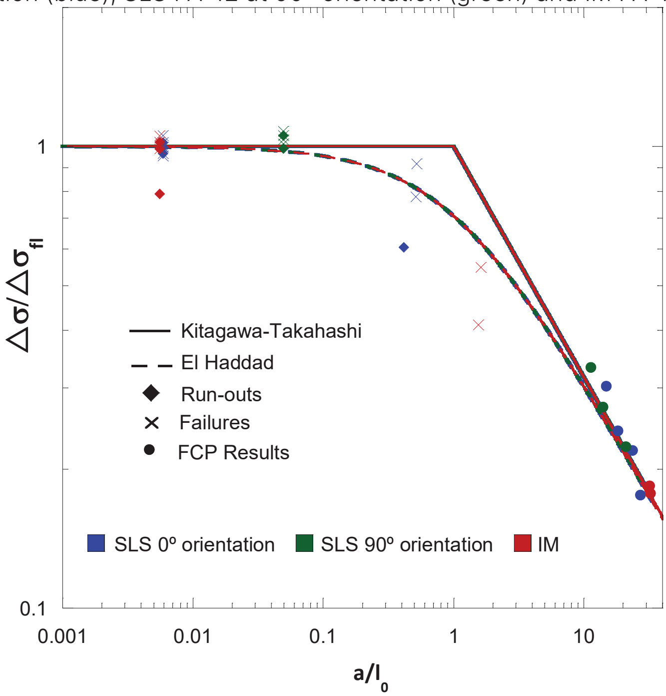

regime, the trend is the opposite, as both *SLS* orientations undergo a better performance than *IM* PA-12. This may be linked to microstructural features. The spherulite size of *SLS* PA-12 is 4 times bigger than that of *IM* PA-12 *(Table 5-3)*, and this could be the reason behind the higher long crack threshold values of the former.

The normalized diagram of *Figure 6-6* displays the complete behaviour of the PA-12 manufactured by different techniques. The stress range has been normalized by the corresponding fatigue limit values at 10^6 cycles for each material and the crack length by their characteristic length.

El Haddad model predictions are more accurate than those of the Kitagawa-Takahashi, especially for *SLS* PA-12. Nevertheless, for *IM* PA-12, El Haddad model does not seem to describe the PSC regime as some failures fall within the integrity zone.

Figure 6-7. Kitagawa-Takahashi diagrams (continuous lines) including El Haddad empirical models (dotted lines) for infinite fatigue lifetime in green and for fracture at one cycle in red of SLS PA12 at 0° orientation: a) full diagrams and b) detail of LC regime with Fatigue Crack Propagation Results obtained from $\Delta\sqrt{G}$-increasing tests.

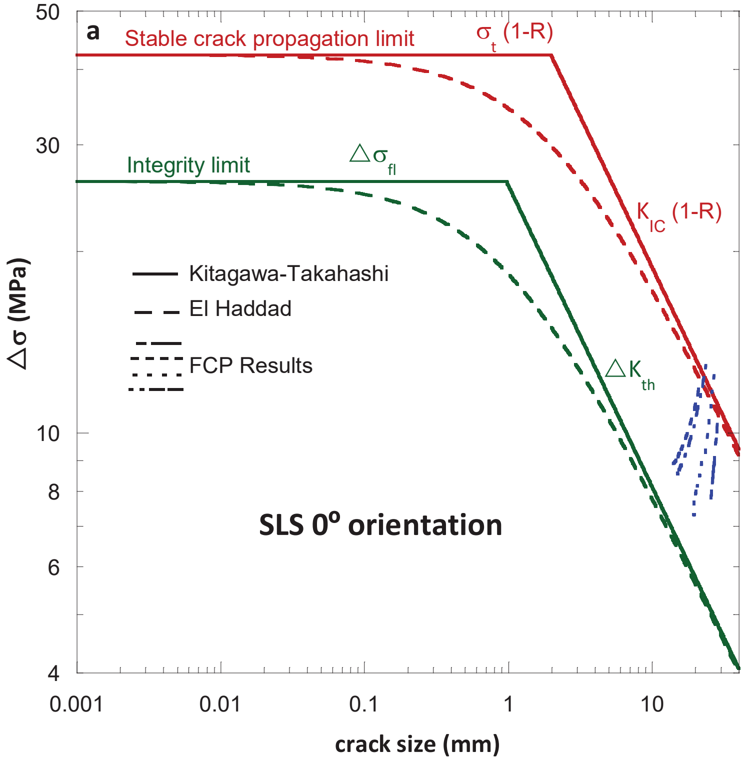

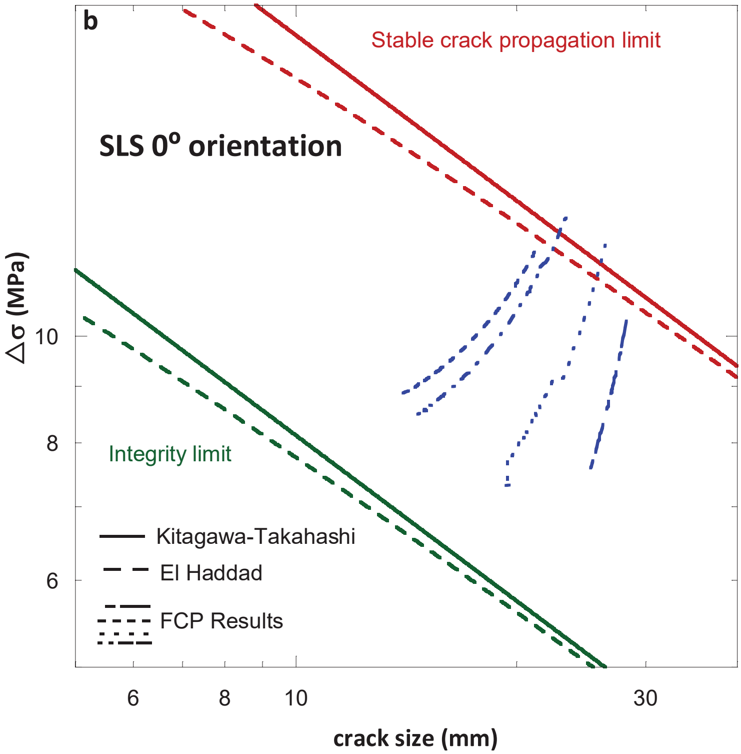

6.3 Finite Fatigue Lifetime

There are several authors (Larsen et al. [180], Ciavarella et al. [181]) who have included in the Kitagawa-Takahashi diagrams the residual strength curves and information about the finite fatigue lifetime. *Figure 6-7, Figure 6-8* and *Figure 6-9* display the Kitagawa-Takahashi diagrams (continuous line) and El Haddad model predictions (dashed line) for static and infinite fatigue lifetime of *SLS* PA- 12 at 0° and 90°orientations, and of *IM* PA-12, respectively.

Red colour is used to represent the static boundary conditions and the infinite fatigue lifetime boundary below which no crack propagates is displayed in green. Between these two limits, finite fatigue life can be predicted by means of a combination of the lifetime fatigue curves and the crack growth propagation curves. In fact, in the LC regime, the Fatigue Crack Propagation curves obtained from $\Delta\sqrt{G}$-increasing tests (*FCP* Results) have been plotted in blue dotted lines.

With the aim of comparing the finite fatigue lifetime band, defined as tensile strength to fatigue limit ratio in *MSC* zone or fracture toughness to long crack threshold in *LC* regime, *Figure 6-10* displays all together the modified

Figure 6-8. Kitagawa-Takahashi diagrams (continuous lines) including El Haddad empirical models (dotted lines) for infinite fatigue lifetime in green and for fracture at one cycle in red of SLS PA12 at 90° orientation: a) full diagrams and b) detail of LC regime with Fatigue Crack Propagation Results obtained from $\Delta\sqrt{G}$-increasing tests.

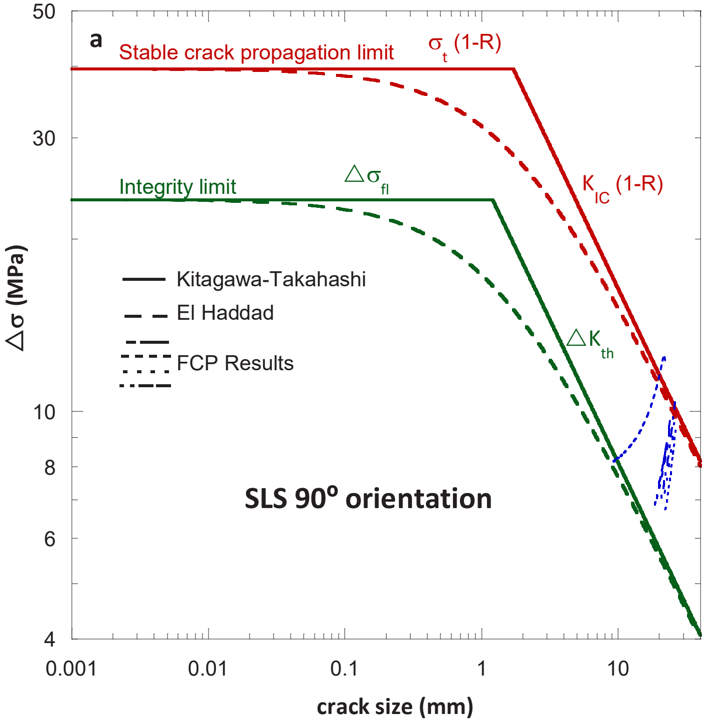

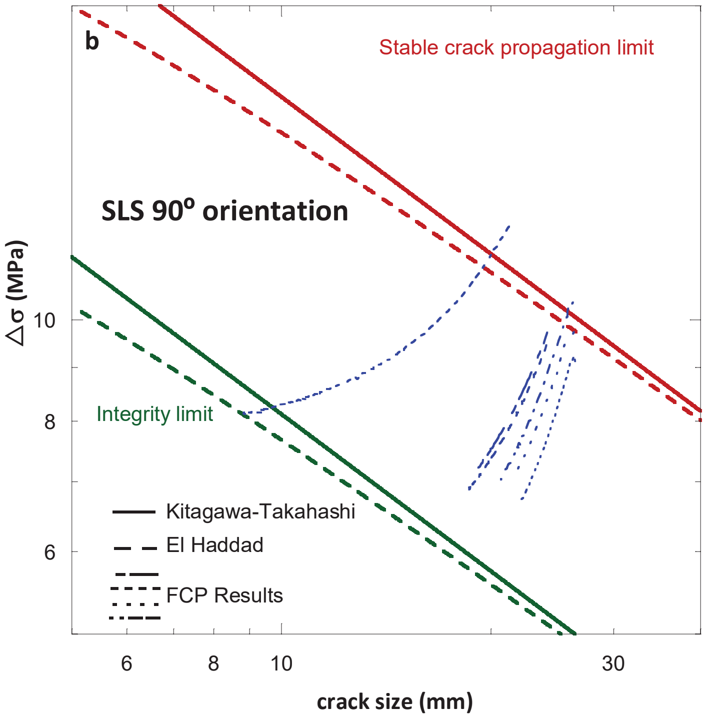

Kitagawa-Takahashi diagrams of *SLS* PA-12 at both orientations and of *IM* PA-12. In metals, the tensile strength to fatigue limit ratio tends to remain roughly constant, independently of the microstructure [182]. This is not the case for these materials. While this ratio holds constant independently of the orientation in *SLS* PA-12, it is reduced for *IM* PA-12. This supports the fact that the band size between these two limiting conditions in the MSC regime seems to be related to the defects population, which are more numerous in *SLS* PA-12.

On the oher hand, in metals, the fracture toughness and the threshold values are closely related to microstructure [182]. In this study, in the *LC* regime, the fracture toughnes to long crack threshold values ratio of *IM* PA-12 was much higher than that of *SLS* PA-12, being hardly differences between 0° and 90° orientations in the former.

The fracture toughness is dependent on the spherulite size, being higher as the spherulite size is smaller, especially appreciated when the fracture values are expressed in terms of the J-integral (*Figure 5-24*). Nevertheless, although the threshold propagation values are lower in *IM* PA-12 and this could be linked to the smaller spherulitic dimension, this topic still needs further investigation.

Ciavarella et al. [181] extended the Kitagawa-Takahashi diagrams for finite life predictions by analogy in the construction of the originals. Therefore, for finite life N, the stress range for each crack length is obtained as the minimum of the stress range resulting from the Basquin law and the integrated form of the Paris law as follows:

$$\Delta\sigma(N,a)=\min\left(\begin{array}{c}\left(\frac{B_B}{N}\right)^{\frac{1}{m_B}},\\ \left(\left(\frac{n-2}{2}\right)A\pi^{\frac{n}{2}}N\right)^{-\frac{1}{n}}a^{\frac{1}{n}-\frac{1}{2}}\end{array}\right) \tag{6-5}$$

In this case, the key issue is the transition from the Basquin dominated regime to the Paris dominated zone, which for a specific number of cycles, N, it is obtained by equating the stress range obtained from the Basquin law and the integrated form of the Paris law. In terms of crack size, l_t, it is given by [181]:

$$l_t(N)=\left(\left(\frac{n-2}{2}\right)A\pi^{\frac{n}{2}}B_B^{\frac{n}{m_B}}N^{m_B-\frac{n}{m_B}}\right)^{\frac{2}{2-n}} \tag{6-6}$$

As a way of example, *Figure 6-11 shows* the fatigue maps including finite life predictions for fatigue lifetimes of 10.000 cycles and 100.000 cycles of *SLS*

Figure 6-9. Kitagawa-Takahashi diagrams (continuous lines) including El Haddad empirical models (dotted lines) for infinite fatigue lifetime in green and for fracture at one cycle in red of IM PA12: a) full diagrams and b) detail of LC regime with Fatigue Crack Propagation Results obtained from $\Delta\sqrt{G}$-increasing tests.

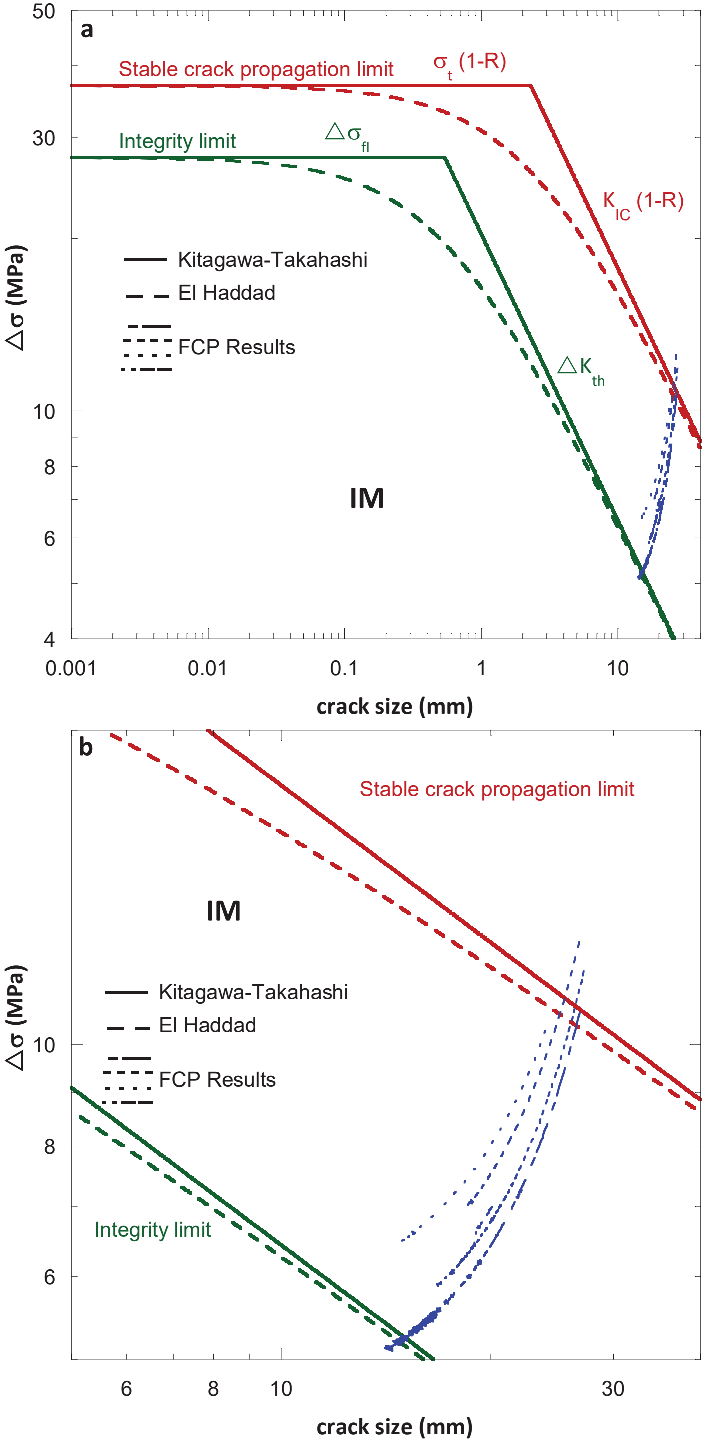

Figure 6-10. Schematic Kitagawa-Takahashi cf SLS PA-12 at 0° orientation in blue, SLS PA-12 at 90° orientation in green and IM PA-12 in red.

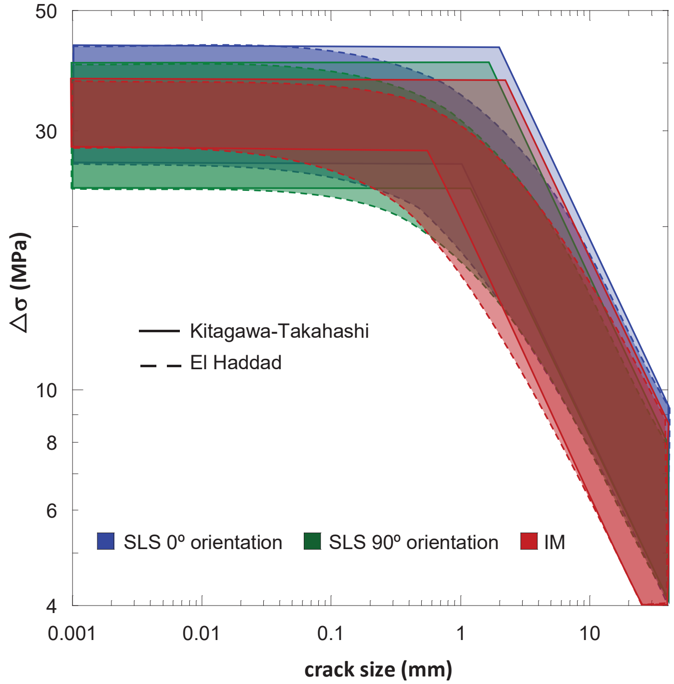

Figure 6-11. Maps of fatigue in normalized coordinates with extended Kitagawa-Takahashi diagrams to finite life with 10.000 cycles in purple and 100.000 cycles in blue between the boundary conditions for fracture and one cycle in red and infinite fatigue life in green of (a) SLS PA-12 at 0° orientation, (b) SLS PA-12 at 90° orientation and (c) IM PA-12.

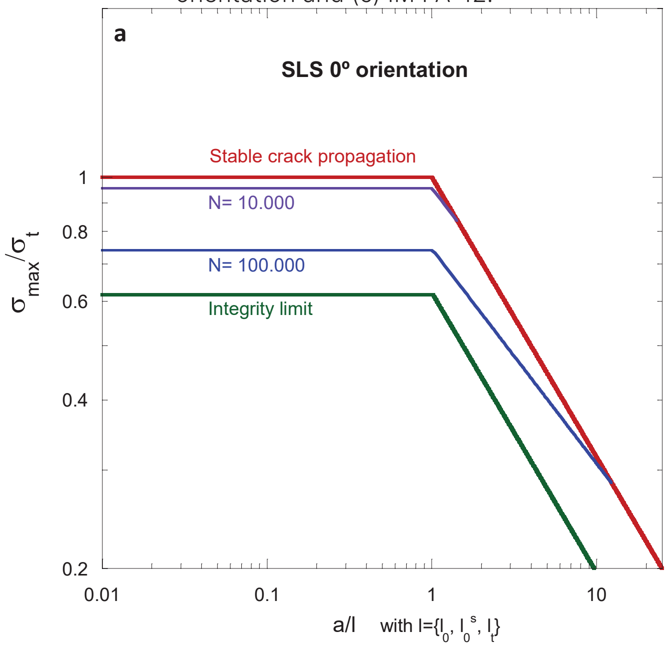

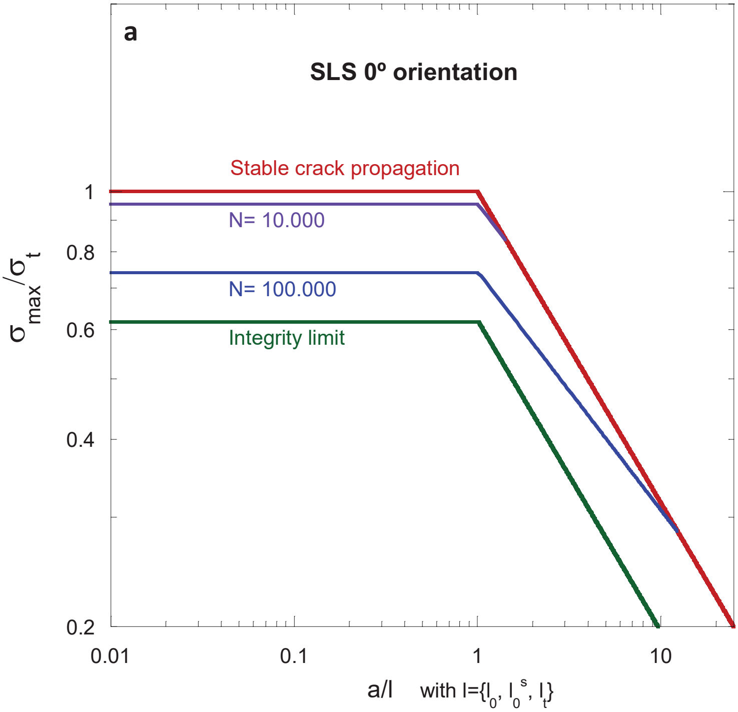
a
SLS 0º orientation
Stable crack propagation
N= 10.000
N= 100.000
Integrity limit
1
0.8
0.6
0.4
0.2
0.01
0.1
1
10
σ_{max}/σ_t
a/l with l={l_0, l_0^s, l_t}

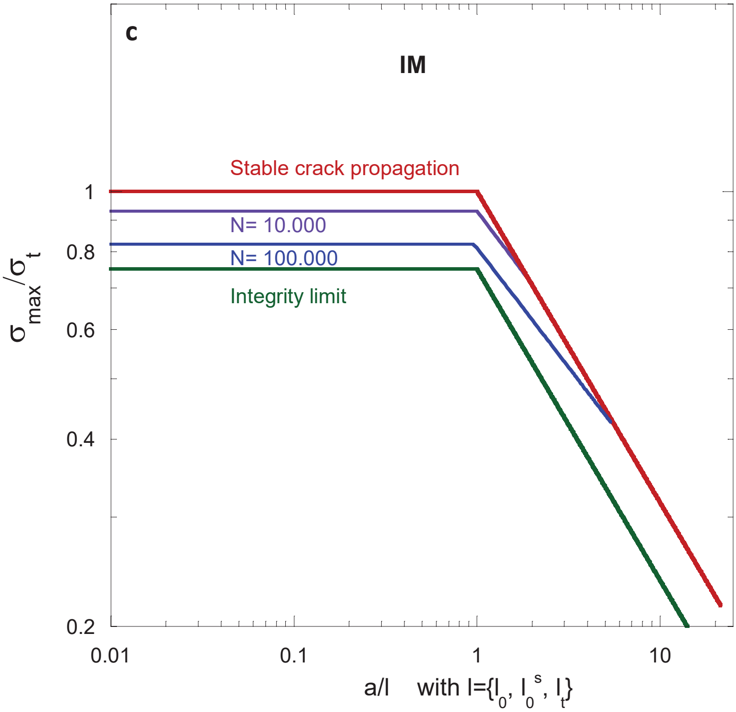
c
IM
Stable crack propagation
N= 10.000
N= 100.000
Integrity limit
1
0.8
0.6
0.4
0.2
0.01
0.1
1
10
σ_{max}/σ_t
a/l with l={l_0, l_0^s, l_t}

PA-12 at 0° and 90°orientations and of *IM* PA-12. Normalized coordinates have been used, that is, the Y-coordinates have been divided by σ_t, and the X-coordinates by l_0^s, $l_t(N)$ or l_0 for static, finite life for a given number of cycles N and infinite life cases, respectively. Little differences were observed among the different materials, only that the region of possible crack propagation is smaller for *IM* PA-12.

6.4 On the physical meaning of l_0

Especially in metals, many authors have tried to give a physical meaning to the characteristic lengths. When the values of l_0 are small, some authors have linked them to microstructural characteristics. El Haddad related them with the crystallographic grain size in steels and titanium alloys [127] and Ciavarella, also in steels, with the distance from the surface to the first microstructural barrier which the crack could found [181]. In other occasions, as in non-metals (building materials, composites or some polymers) or in materials with no microstructure because they are amorphous, the characteristic length can be associated with the size of the damage zone. In this case, the characteristic length can range from only some hundreds of microns to millimetres, being mostly at least one order of magnitude larger than the microstructural features as there can be many factors involved in the creation and growth of the damage.

For the materials under study, the characteristic lengths could be associated neither with any microstructure feature (spherulite size, skin layer dimension, surface roughness, etc) nor with damage zone size. Therefore, further research should be done in this topic to elucidate if the values of l_0 obtained could be related to material properties or failure processes.